Journal of Nuclear Materials 396 (2010) 163–169

Contents lists available at ScienceDirect

Journal of Nuclear Materials

journal homepage: www.elsevier.com/locate/jnucmat

Resolving the H_2 effect on radiation induced dissolution of UO_2-based spent nuclear fuel

Martin Trummer, Mats Jonsson *

KTH Chemical Science and Engineering, Nuclear Chemistry, Royal Institute of Technology, SE-100 44 Stockholm, Sweden

ARTICLE INFO

Article history:
Received 19 August 2009
Accepted 31 October 2009

Keywords:
Spent nuclear fuel
Dissolution
Radiolysis
H_2 effect
Simulation

ABSTRACT

In recent years, the impact of H_2 on α-radiation induced dissolution of UO_2-based spent nuclear fuel has been studied and debated extensively. Experimental results on the effect of H_2 on the concentration of H_2O_2 during α-radiolysis have been shown to disagree with numerical simulations. For this reason, the reaction scheme used in simulations of aqueous radiation chemistry has sometimes been questioned.

In this work, we have studied the impact of H_2 on the H_2O_2 concentration in α-irradiated aqueous solution using numerical simulations. The effects of H_2 pressure, α-dose rate and HCO_3^- concentration were investigated by performing systematic variations in these parameters. The simulations show that the discrepancy between the previously published experimental result and numerical simulations is due to the use of a homogeneous dose rate (the energy is assumed to be equally distributed in the whole volume). Taking the actual dose rate of the α-irradiated volume into account, the simulation is in perfect agreement with the experimental results. This shows that the H_2 effect is strongly α-dose rate dependent, and proves the reliability of the reaction scheme used in the simulations.

The simulations also show that H_2 influences the H_2O_2 concentration under α-radiolysis. The magnitude of the effect depends on the dose rate and the H_2 pressure as well as on the concentration of HCO_3^-. The impact of the radiolytic H_2 effect on the rate of α-radiation induced dissolution of spent nuclear fuel is discussed along with other (α- and γ-) radiation induced processes capable of reducing the concentration of uranium in solution. The radiolytic H_2 effect is quantitatively compared to the previously presented noble metal catalyzed H_2 effect. This comparison shows that the noble metal catalyzed H_2 effect is far more efficient than the radiolytic H_2 effect. Reduction of U(VI) in solution due to low dose rate γ-radiolysis in the presence of H_2 is proposed to be the cause of the H_2 effect observed in leaching experiments on α-doped UO_2.

1. Introduction

Understanding the mechanism behind radiation induced dissolution of spent nuclear fuel is a prerequisite for reliable safety assessments of deep geological repositories for spent nuclear fuel. In such repositories, the radioactive waste will be protected from the groundwater by a system of multiple barriers where the fuel matrix (UO_2) itself constitutes the innermost barrier [1]. Under the conditions expected in deep granitic groundwaters, the solubility of UO_2 is very low [2]. However, the inherent radioactivity of the spent nuclear fuel will induce decomposition (radiolysis) of water into redox reactive species capable of altering the groundwater conditions in the vicinity of the UO_2 surface. Oxidation of the UO_2-matrix leads to production of more readily soluble U(VI)-species and thereby to matrix dissolution accompanied by the release of radiotoxic fission products and actinides. The oxidizing species produced by radiolysis of water are $OH^{\cdot}$, H_2O_2, O_2 and $HO_2^{\cdot}$ [3]. In the presence of HCO_3^-, $OH^{\cdot}$ is converted to $CO_3^{\cdot-}$ which is also a strong oxidant. All these oxidants are capable of oxidizing UO_2 to U(V) or U(VI) rendering a potentially complex reaction system. However, recent studies have shown that H_2O_2 is responsible for virtually 100% of the UO_2 oxidation under deep repository conditions [4]. This finding simplifies predictive modeling of the dynamics of spent nuclear fuel dissolution significantly. A fairly simple but useful approach is to use the steady-state approximation, i.e. that the rate of H_2O_2 consumption is equal to the rate of H_2O_2 production by radiolysis [5]. In a system where dissolution of oxidized UO_2 is not a limitation and in the absence of solutes reactive towards H_2O_2, the main route for H_2O_2 consumption is by reaction with the UO_2 surface, and the rate of UO_2-matrix dissolution can be calculated from the dose rate and the radiation chemical yield (*G*-value) [6].

While the dynamics of radiation induced oxidative dissolution of UO_2 can be considered to be well understood, the effect of H_2 (produced by radiolysis of water and anaerobic corrosion of iron

* Corresponding author. Tel.: +46 8 790 9123; fax: +46 8 790 8772.
E-mail address: matsj@kth.se (M. Jonsson).

0022-3115/$ - see front matter © 2009 Elsevier B.V. All rights reserved.
doi:10.1016/j.jnucmat.2009.10.067

containing canisters) is still not clear [7]. Several studies have shown that radiation induced dissolution of spent nuclear fuel is effectively inhibited in the presence of H_2 [8,9]. The inhibition is expressed in terms of low concentrations of uranium as well as of less redox sensitive radionuclides. This implies that the oxidative dissolution is indeed stopped. In addition, the concentration of H_2O_2 reaches a constant steady-state level also in the presence of H_2. This indicates that H_2O_2 is consumed in the system, either by a surface reaction or by a reaction occurring in the bulk. On the basis of electrochemical and kinetic studies on model systems, a mechanism accounting for the observed H_2 effect has been proposed [5,10,11]. In this mechanism, noble metal inclusions (ε-phase particles) catalyze the H_2 reduction of U(VI) on the fuel surface back to U(IV). This mechanism accounts both for the inhibited dissolution and the apparent H_2O_2 consumption (Scheme 1).

Using the rate constant for the noble metal catalyzed reduction (obtained from kinetic studies [11]), it is possible to simulate the effect of H_2 on spent nuclear fuel dissolution with high accuracy [12].

In addition to the H_2 effect observed in experiments on spent nuclear fuel, inhibition has also been seen in experiments using α-doped UO_2 [13,14]. Unlike spent nuclear fuel, α-doped UO_2 does not contain noble metal inclusions as these are composed of fission products originating from the energy production. Consequently, the mechanism presented in Scheme 1 does not provide an explanation for the observed H_2 effect in the case of α-doped UO_2.

Indeed, the fairly complex reaction scheme for water undergoing radiolysis can provide some additional insights [15]. The following reactions reduce the H_2O_2 concentration in the presence of H_2.

$$OH^{\cdot} + H_2 \rightarrow H_2O + H^{\cdot} \quad (1)$$

$$H^{\cdot} + H_2O_2 \rightarrow H_2O + OH^{\cdot} \quad (2)$$

This chain reaction becomes efficient when the H_2 concentration is sufficiently high (compared to the H_2O_2 concentration). The hydroxyl radical also reacts with H_2O_2. However, this is not a chain reaction.

In addition, quantitative conversion of oxidizing hydroxyl radicals into reducing hydrogen atoms can influence already dissolved U(VI) by reducing it back to the much less soluble U(IV) according to the following reactions [16–18].

$$H^{\cdot} + U(VI) \rightarrow H^{+} + U(V) \quad (3)$$

$$H^{\cdot} + U(V) \rightarrow H^{+} + U(IV) \quad (4)$$

$$U(V) + U(V) \rightarrow U(VI) + U(IV) \quad (5)$$

Consequently, aqueous radiation chemistry could also provide an explanation for the observed H_2 effect in the absence of noble metal particles.

In 2001, Pastina and LaVerne published a study on the effect of molecular hydrogen on hydrogen peroxide production in water radiolysis [19]. The experimental results presented in this study showed that 800 μM H_2 has virtually no effect on the production of H_2O_2 during α-radiolysis (α-radiation being the most important type of radiation under deep repository conditions). On the other hand, numerical simulations presented in the same paper predict a strongly inhibiting effect of H_2. The buildup of oxidizing species was argued to be one possible explanation for this discrepancy [19]. This inconsistency obviously caused confusion and prompted scientists in the field of spent nuclear fuel dissolution to question the reliability of the reaction scheme used in the numerical simulations of water radiolysis. This also opened up for alternative explanations involving surface catalyzed reduction by H_2 [7].

In the experiment performed by Pastina and LaVerne, 20 mL solutions were irradiated with 5 MeV $^4He^{2+}$ particles from an accelerator. The penetration depth of the accelerated ions in water is in the order of 40 μm. Hence, only a very small fraction of the solution volume is actually exposed to radiation. In the numerical simulations performed, the system is homogenized, i.e. the radiation energy is assumed to be homogeneously absorbed by the whole volume. As a consequence, the actual dose rate in the experiment is several orders of magnitude higher than the dose rate used in the simulation. This discrepancy is a plausible cause for the apparent disagreement between the experimental results and the numerical simulation.

In this study we have investigated the effect of H_2 on radiolytic production of H_2O_2 as a function of dose rate and HCO_3^- concentration in order to resolve the origin of the observed H_2 effect. The investigation is based on numerical simulations.

The combined effect of radiolysis and H_2 on U(VI) in solution is also studied to some extent for both α- and γ-radiation.

2. Simulations

Numerical simulations of α- and γ-radiolysis of water were performed using MAKSIMA-Chemist [20]. The reactions and the corresponding rate constants employed are presented in Table 1. The *G*-values used are presented in Table 2.

The last reaction in Table 1 is used to make a homogeneous representation of the surface reaction between H_2O_2 and UO_2 leading to dissolution of uranium (in cases where the UO_2 system is simulated). The homogeneous first order rate constant is calculated

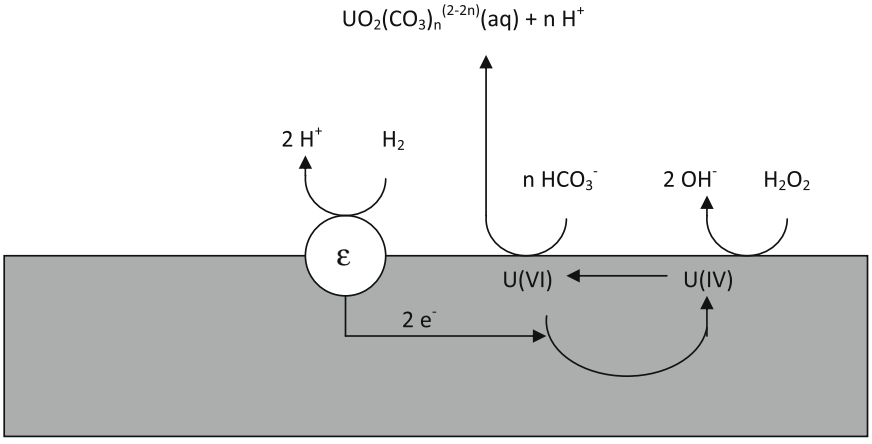

Scheme 1. Elementary processes involved in radiation induced oxidative dissolution of spent nuclear fuel.

Table 1
Reaction scheme used in MAKSIMA simulations.

Reaction	Rate const.[a]
$OH^{\cdot} + OH^{\cdot} = H_2O_2$	4.000×10^9
$OH^{\cdot} + e^- = OH^- + H_2O$	2.000×10^{10}
$OH^{\cdot} + H^{\cdot} = H_2O$	2.500×10^{10}
$OH^{\cdot} + O_2^- = OH^- + O_2$	1.000×10^{10}
$OH^{\cdot} + H_2O_2 = H_2O + O_2^- + H^+$	2.250×10^7
$OH^{\cdot} + H_2 = H_2O + H^{\cdot}$	4.000×10^7
$e^- + e^- = OH^- + OH^- + H_2$	5.000×10^9
$e^- + H^{\cdot} = OH^- + H_2$	2.000×10^{10}
$e^- + HO_2^{\cdot} = HO_2^- + H_2O$	2.000×10^{10}
$e^- + O_2^- = HO_2^- + OH^-$	1.200×10^{10}
$e^- + H_2O_2 = OH^{\cdot} + OH^- + H_2O$	1.600×10^{10}
$e^- + H^+ = H^{\cdot} + H_2O$	2.200×10^{10}
$e^- + O_2 = O_2^- + H_2O$	2.000×10^{10}
$e^- + H_2O = H^{\cdot} + OH^- + H_2O$	2.000×10^1
$H^{\cdot} + H^{\cdot} = H_2$	1.000×10^{10}
$H^{\cdot} + HO_2^{\cdot} = H_2O_2$	2.000×10^{10}
$H^{\cdot} + O_2^- = HO_2^-$	2.000×10^{10}
$H^{\cdot} + H_2O_2 = OH^{\cdot} + H_2O$	6.000×10^7
$H^{\cdot} + OH^- = e^-$	2.000×10^7
$H^{\cdot} + O_2 = O_2^- + H^+$	2.000×10^{10}
$HO_2^{\cdot} = O_2^- + H^+$	8.000×10^5
$HO_2^{\cdot} + HO_2^{\cdot} = O_2 + H_2O_2$	7.500×10^5
$HO_2^{\cdot} + O_2^- = O_2 + HO_2^-$	8.500×10^7
$O_2^- + H^+ = HO_2^{\cdot}$	5.000×10^{10}
$H_2O_2 + OH^- = HO_2^- + H_2O$	5.000×10^8
$HO_2^- + H_2O = H_2O_2 + OH^-$	5.735×10^4
$H_2O = H^+ + OH^-$	2.599×10^{-5}
$H^+ + OH^- = H_2O$	1.430×10^{11}
$OH^{\cdot} + CO_3^{2-} = CO_3^{\cdot-} + OH^-$	4.000×10^8
$OH^{\cdot} + HCO_3^- = CO_3^{\cdot-} + H_2O$	1.500×10^7
$O_2^- + CO_3^{\cdot-} = CO_3^{2-} + O_2$	3.200×10^8
$H_2O_2 + CO_3^{\cdot-} = CO_3^{2-} + O_2^- + H^+ + H^+$	4.300×10^5
$HO_2^- + CO_3^{\cdot-} = CO_3^{2-} + O_2^- + H^+$	3.000×10^7
$H^+ + HCO_3^- = CO_2 + H_2O$	1.000×10^{10}
$OH^- + HCO_3^- = CO_3^{2-} + H_2O$	1.000×10^9
$H_2O + CO_2 = HCO_3^- + H^+$	8.410×10^1
$H_2O + CO_3^{2-} = HCO_3^- + OH^-$	3.800×10^3
$H_2O + CO_4^{2-} = CO_3^{2-} + H_2O_2$	2.000×10^{-1}
$CO_3^- + CO_3^- = CO_4^{2-} + CO_2$	7.000×10^6
$O_2^- + O_2^- = HO_2^- + O_2$	3.500×10^{-1}
$e^- + CO_3^{\cdot-} = CO_3^{2-}$	1.000×10^{10}
$H^{\cdot} + CO_3^{\cdot-} = HCO_3^-$	1.000×10^{10}
$U(VI) + e^- = U(V)$	1.000×10^{10} [21]
$U(VI) + H^{\cdot} = U(V)$	1.000×10^{10}[b]
$U(V) + U(V) = U(IV) + U(VI)$	1.000×10^{3}[b]
$U(V) + e^- = U(IV)$	1.000×10^{10}[b]
$U(V) + H^{\cdot} = U(IV)$	1.000×10^{10}[b]
$H_2O_2 = U(VI)$	2.086×10^{-3} [22]

[a] Ref. [15] unless otherwise stated.
[b] Adopted from Refs. [16–18] taking pH-effects into account.

from the heterogeneous rate constant presented in Ref. [22] by assuming that the volume is limited by the maximum α-range. By multiplying the heterogeneous rate constant with the surface area to solution volume ratio (given by the inverse of the maximum α-range), the system specific first order rate constant is obtained. The rate constants for the reactions responsible for reduction of U(VI) in solution have been determined under different conditions from those used in the simulations. The rate constants for the reactions between e^-_{aq} and oxidized uranium are believed to be reliable while the reaction involving the hydrogen atom and oxidized uranium are somewhat more uncertain. In the simulations, the dose rate was varied between 0.000544 and 0.595 Gy s^{-1}, the H_2 concentration was varied between 0 and 30 mM and the HCO_3^- concentration was varied between 0 and 10 mM. The dose rates were chosen to mimic spent nuclear fuel (burn-up 38 MWd/kg U) of ages 100–100,000 years [25]. The highest dose rate corresponds to fuel considerably younger than 100 years.

3. Results and discussion

In the experiment performed by Pastina and LaVerne [19], the H_2 concentration is 800 μM (1 bar) and the initial H_2O_2 concentration is 50 μM. The homogeneous dose rate is 0.25 Gy s^{-1}, and the total solution volume is 20 mL. According to previous publications on the same experimental set up, the cross section of the ion beam is 0.3 cm^2 [26]. Taking into account that the penetration depth for 5 MeV α-particles is ca. 40 μm, the irradiated volume is calculated to 1.2 μL. Hence, the dose rate in the irradiated volume is more than four orders of magnitude higher than the homogenized dose rate. Numerical simulations performed using both the homogenous dose rate and the actual dose rate in the irradiated volume are presented in Fig. 1.

As can be seen, the simulation performed using the homogeneous dose rate displays a significant H_2 effect while the simulation performed using the actual dose rate in the irradiated volume shows no sign of inhibition by H_2. The latter simulation is in perfect agreement with the experimental finding by Pastina and LaVerne. This finding clearly shows that the radiolytic reaction scheme used in most simulations is indeed reliable. Judging from our results, the effect of H_2 on the concentration of radiolytically produced H_2O_2 is strongly dose rate dependent.

The dose rate in the irradiated volume of the experiment discussed above is several orders of magnitude higher than the dose rates of relevance in a deep repository for spent nuclear fuel [25]. Therefore, we have performed a series of simulations using α-dose rates expected to be relevant under deep repository conditions. As stated above, we have systematically varied the H_2- and HCO_3^--concentrations. In Fig. 2, the H_2O_2 concentration as a function of irradiation time is plotted for different H_2 concentrations at the highest dose rate used in the simulations (0.595 Gy s^{-1}).

As can be seen, the H_2O_2 concentration is suppressed in the presence of H_2. At the highest dose rate (Fig. 2), a H_2 pressure higher than 0.01 bar (8 μM) is required to influence the H_2O_2 concentration. From the simulations, it is also obvious that the H_2 pressure required to suppress the H_2O_2 concentration decreases with decreasing dose rate. When simulating longer irradiation times, it becomes clear that the H_2O_2 concentration reaches a steady-state level in the cases where H_2 displays an effect. By performing a series of simulations at different H_2 pressures, we were able to pin point the critical H_2 pressures at which suppression of the H_2O_2 concentration occurs. In Fig. 3 the critical H_2 pressure is plotted as a function of α-dose rate.

It is obvious that the critical H_2 pressure increases with increasing dose rate, and that very low H_2 pressures affect the H_2O_2 concentration at dose rates relevant in the safety assessment of deep geological repositories for spent nuclear fuel. It should be noted

Table 2
G-values used in the MAKSIMA calculations.

Radiation	$G(H_2O)$	$G(H_2)$	$G(H_2O_2)$	$G(e^-_{aq})$ μmol J^{-1}	$G(H^{\cdot})$	$G(^{\cdot}OH)$	$G(HO_2^{\cdot})$
α [23]	−0.281	0.135	0.102	0.0062	0.022	0.025	0.023
γ [24]	−0.430	0.047	0.073	0.28	0.062	0.28	0.0027

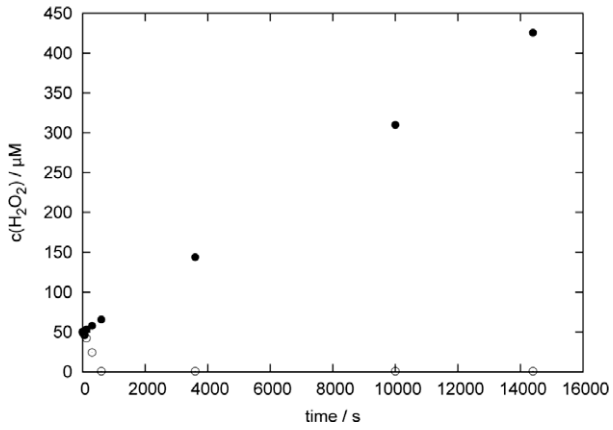

Fig. 1. H_2O_2 concentration as a function of irradiation time for the homogeneous (○, 0.25 Gy s^{-1}) and actual (●, 1667 Gy s^{-1}) dose rates in the experiment by Pastina and LaVerne [19].

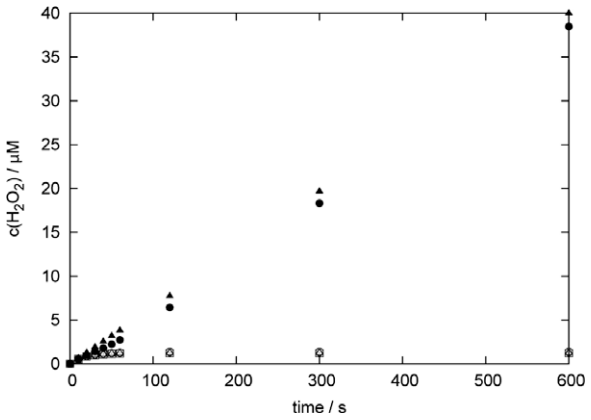

Fig. 2. H_2O_2 concentration vs. irradiation time at 0 (▲), 7.63×10^{-6} (●), 7.63×10^{-5} (○), 7.63×10^{-4} (□), 7.63×10^{-3} (◇) and 3.05×10^{-2} (△) M H_2 (0.595 Gy s^{-1}).

that the common method of homogeneously diluting the dose in a volume larger than the one actually being exposed to α-radiation used in many numerical simulations, will overestimate the H_2 effect due to the dose rate dependence. Using the dose rate dependence illustrated in Fig. 3, we calculate the critical H_2 pressure in the experiment by Pastina and LaVerne [19] to 2.7 bar (ca. 2 mM). This is considerably higher than the H_2 pressure used in the experiment.

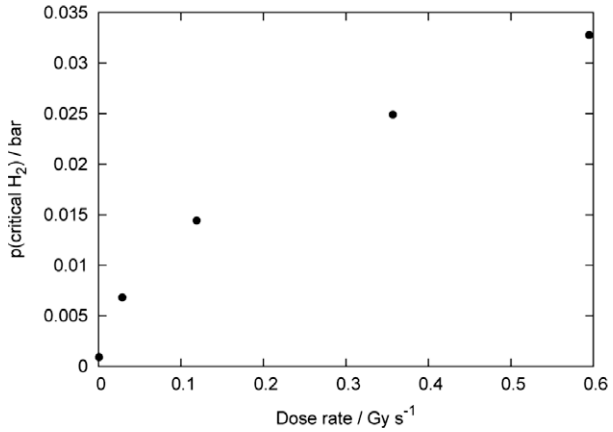

Fig. 3. Critical H_2 pressure vs. dose rate at 0 mM HCO_3^-.

The H_2O_2 steady-state levels obtained in the simulations display a strong dependence on the dose rate and a weak dependence on the H_2 pressure. At a given H_2 pressure the steady-state concentration is proportional to the square root of the dose rate while at a given dose rate the steady-state concentration is inversely proportional to the H_2 pressure. The steady-state concentration of hydrogen atom, the reactant responsible for the H_2O_2 suppression, increases with increasing H_2 pressure $\left([H]_{S-S} \propto -\frac{1}{pH_2}\right)$ and is proportional to the square root of the dose rate. As reaction (2) is the main reaction responsible for consumption of H_2O_2, the rate of H_2O_2 consumption will be proportional to the hydrogen atom steady-state concentration and thereby to the square root of the dose rate ($\dot{D}$). The rate of H_2O_2 production is proportional to the dose rate, and the H_2O_2 steady-state concentration will therefore be proportional to the ratio between the dose rate and the square root of the dose rate according to Eq. (6)

$$[H_2O_2]_{S-S} = \frac{c_1\dot{D}}{c_2\sqrt{\dot{D}}} = \frac{c_1}{c_2}\sqrt{\dot{D}} \tag{6}$$

where c_1 and c_2 are constants. The square root dependence for the hydrogen atom steady-state concentration is a result of the self-recombination reaction being the main route for radical consumption.

3.1. Effect of HCO_3^-

Most groundwaters contain HCO_3^- in mM concentrations. In the presence of HCO_3^-, the radiolytically produced hydroxyl radical is scavenged according to reaction (7).

$$OH^{\cdot} + HCO_3^- \rightarrow H_2O + CO_3^{\cdot-} \tag{7}$$

In the presence of H_2, reactions (1) and (7) will compete, and the inhibiting effect of H_2 is therefore expected to decrease with increasing HCO_3^- concentration. This is also revealed by the simulations. Interestingly, the relative dose dependence on the critical H_2 pressure decreases with increasing HCO_3^- concentration and the critical H_2 pressure virtually becomes a function of the HCO_3^- concentration. The critical H_2 pressure is plotted as function of HCO_3^- concentration in Fig. 4.

It is also interesting to note that the H_2O_2 steady-state concentrations obtained above the critical H_2 pressures in the presence of HCO_3^- are slightly lower than the corresponding H_2O_2 steady-state concentrations in the absence of HCO_3^-. The rationale for this is simply a pH effect which can be verified by performing a simulation on a HCO_3^- free system using the pH of a HCO_3^- containing system.

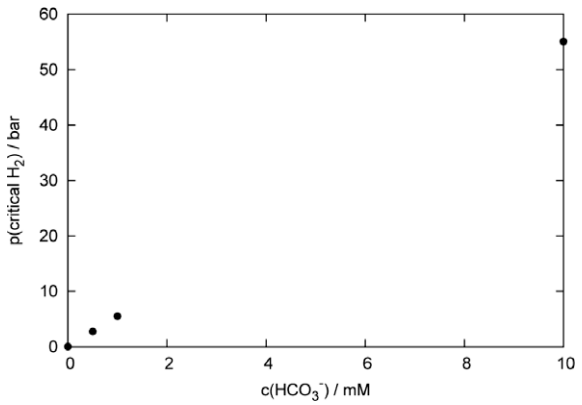

Fig. 4. Critical H_2 pressure vs. HCO_3^- concentration (0.595 Gy s^{-1}).

3.2. The H_2 effect on radiation induced oxidative dissolution of UO_2

In UO_2 and spent nuclear fuel leaching experiments, the concentration of uranium in solution is the key observable. This observable depends on both the H_2O_2 production from radiolysis and redox reactions in solution producing less soluble forms of uranium. H_2 reacts very slowly with U(VI) in solution [27]. However, in the presence of a catalyst, the reaction is considerably faster [28]. The combined effect of ionizing radiation and H_2 on U(VI) in solution is accounted for in reactions (3)–(5). To demonstrate the impact of the radiolytic H_2 effect, we performed simulations taking UO_2 oxidation and reactions (3)–(5) into account. The resulting logarithmic uranium concentration vs. irradiation time plot is given in Fig. 5.

As can be seen, the radiolytic H_2 effect is sufficient to suppress the uranium concentration in solution. In this particular case, the α-dose rate is 0.595 Gy s^{-1}, the H_2 pressure is 40 bar and the HCO_3^- concentration is 1 mM. However, it should be stressed that reactions (3)–(5) do not inhibit the release of radionuclides from spent nuclear fuel. These reactions merely account for reduction of U(VI) in solution. For this reason, a simulation where these reactions are excluded is also illustrated in Fig. 5. The simulation clearly shows that reactions (3)–(5) are responsible for the major part of the observed effect. Hence, even though the uranium concentration in solution is very low, the rate of matrix dissolution is still significant although the rate of dissolution is reduced by approximately one order of magnitude.

When including the radiation induced reactions responsible for reduction of U(VI) to U(IV), the U(VI) as well as the H_2O_2 concentrations reach steady-state. This is illustrated in Fig. 6.

Under these conditions, the rate of H_2O_2 production is equal to the rate of H_2O_2 consumption, and the rate of UO_2 oxidation is equal to the rate of U(VI) reduction. As the rate of UO_2 oxidation depends on the H_2O_2 concentration, all four reactions are interconnected and dependent on the dose rate. It is important to note that steady-state with respect to H_2O_2 is not the only prerequisite for a steady-state with respect to U(VI) in solution. At H_2O_2 steady-state, the rate of UO_2 oxidation is constant. To obtain steady-state with respect to U(VI), a sufficiently high concentration of hydrogen atoms must be available. As stated above, the steady-state concentration of hydrogen atoms increases with increasing dose rate. For this reason, a certain dose rate is required to obtain steady-state with respect to U(VI). The critical dose rate above which steady-state is reached is around 0.27 Gy s^{-1} at 40 bar H_2 and in the absence of HCO_3^-. The critical value increases with decreasing H_2 pressure and with increasing HCO_3^- concentration. In Fig. 7, the

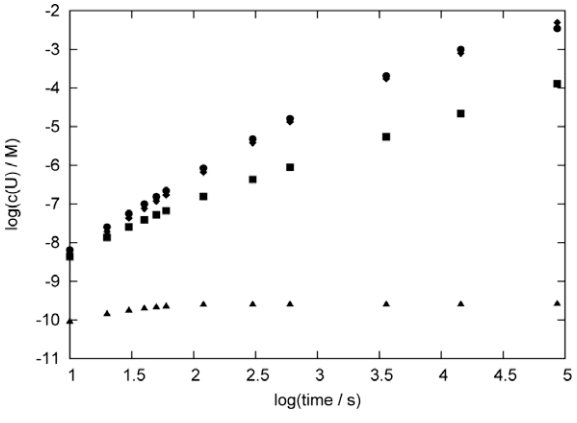

Fig. 5. Logarithmic plot of U(VI) concentration vs. irradiation time at 40 bar H_2 and under inert atmosphere, with and without U(VI) reduction taken into account (inert – reduction (♦), inert – no reduction (●), H_2 – reduction (▲), H_2 – no reduction (■)).

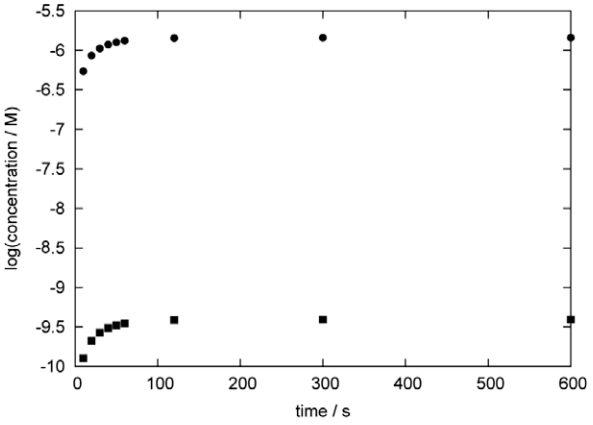

Fig. 6. Logarithm of H_2O_2 (●) and U(VI) (■) concentration plotted against irradiation time (U(VI) reduction included).

U(VI) steady-state concentrations are plotted against HCO_3^- concentration for 1, 10 and 40 bar H_2 at a dose rate of 0.595 Gy s^{-1}. At HCO_3^- concentrations beyond the last point in each series, the U(VI) concentration does not reach steady-state.

It is evident that the steady-state concentration of U(VI) is always below 1 nM in this particular system, i.e. radiation induced dissolution of UO_2 would appear to be completely inhibited. The HCO_3^- concentration range within which U(VI) steady-state can be reached increases with increasing H_2 pressure. At 40 bar H_2, more than 2 mM HCO_3^- can be present, and the U(VI) concentration still approaches a very low steady-state level. However, it should be emphasized that the α-dose rates above which U(VI) steady-state is reached are higher than would be expected in a deep repository for spent nuclear fuel under the conditions relevant for a safety assessment.

3.3. Radiolytic H_2 effect vs. noble metal catalyzed H_2 effect

From a more practical point of view, it is of interest to compare the magnitude of the two H_2 effects on radiation induced oxidative dissolution of spent nuclear fuel. The effect of the noble metal catalyzed inhibition is quantitatively described by Eq. (8) [5,11]

$$r_{diss} = r_{ox} - k\varepsilon_{rel}[H_2] \quad (8)$$

where r_{diss} is the rate of oxidative UO_2 dissolution, r_{ox} is the uninhibited rate of UO_2 oxidation, k (=10^{-6} m s^{-1} [11]) is the rate constant

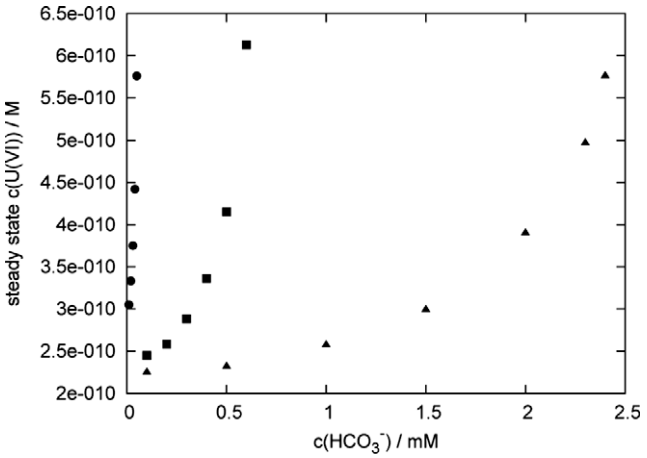

Fig. 7. Steady-state concentration of U(VI) at 1 (●), 10 (■) and 40 (▲) bar H_2 plotted as a function of HCO_3^- concentration.

Table 3
Critical H_2 concentrations in the noble metal catalyzed and radiolytic H_2 effects.

Dose rate	$c(H_2(\varepsilon))$	Critical $c(H_2$(0 mM HCO_3^-))mol dm^{-3}	Critical $c(H_2$(1 mM HCO_3^-))
0.000544	4.99×10^{-10}	$\sim 7.00 \times 10^{-7}$	4.10×10^{-3}
0.0059	5.41×10^{-9}	$\sim 2.35 \times 10^{-6}$	4.12×10^{-3}
0.0287	2.63×10^{-8}	$\sim 5.28 \times 10^{-6}$	4.14×10^{-3}
0.119	1.09×10^{-7}	$\sim 1.10 \times 10^{-5}$	4.17×10^{-3}
0.357	3.27×10^{-7}	$\sim 1.93 \times 10^{-5}$	4.20×10^{-3}
0.595	5.46×10^{-7}	$\sim 2.50 \times 10^{-5}$	4.22×10^{-3}

for the noble metal catalyzed reduction of U(VI) to U(IV) by H_2, ε_{rel} is the fraction of the surface area covered by noble metal particles, and $[H_2]$ is the hydrogen concentration in solution. Assuming the noble metal particle surface coverage to be 1%, we can calculate the H_2 pressure or concentration required to completely cancel the oxidative dissolution of UO_2 ($r_{diss} = 0$). In Table 3, these values are given along with critical values for the radiolytic H_2 effect (at 0 and 1 mM HCO_3^-) for the α-dose rates used in this work.

As can be seen, the noble metal catalyzed H_2 effect is significantly more powerful in all cases. Furthermore, it should be kept in mind that the critical values for the radiolytic H_2 effect do not correspond to complete cancellation of the oxidative UO_2 dissolution.

3.4. Accounting for the radiolytic H_2 effect in predictive modeling of spent nuclear fuel dissolution

As shown above, the impact of the radiolytic H_2 effect depends on the α-dose rate. For this reason, homogeneous models are bound to fail since the dose rate displays a strong variation with distance from the fuel surface. The only way to accurately account for this effect is by performing simulations taking the geometrical dose distribution into account. Such simulations are very tedious, and it is difficult to simulate longer irradiation times of relevance in the safety assessment of deep repositories. On the other hand, since the noble metal catalyzed inhibition is much more efficient, the radiolytic H_2 effect can be neglected for spent nuclear fuel, thus simplifying the simulations significantly.

To mimic experiments using α-doped UO_2, the radiolytic H_2 effect must be accounted for. As stated above, the steady-state concentration of H_2O_2 depends on the H_2 pressure as well as the dose rate. The steady-state concentrations obtained as a result of the radiolytic H_2 effect are in most cases lower than the corresponding steady-state concentrations expected from the previously mentioned steady-state approach for radiation induced dissolution of UO_2 (calculated from Eq. (9) [5]).

$$[H_2O_2]_{S-S} = \frac{\dot{D} G(H_2O_2) \rho \delta_{\max}(\alpha)}{k_{H_2O_2}} \tag{9}$$

The expression in the numerator of Eq. (9) gives the rate of H_2O_2 production per m^2 UO_2 surface. In the equation, $\dot{D}$ is the average α-dose rate in the irradiated volume, $G(H_2O_2)$ is the radiation chemical yield of H_2O_2, ρ is the density of water, $\delta_{\max}(\alpha)$ is the maximum range of the α-particles in water, and $k_{H_2O_2}$ is the rate constant for the reaction between H_2O_2 and the UO_2 surface. Hence, the steady-state concentration in the system will be governed by the radiolytic effect. In Table 4, the ratio between the H_2O_2 steady-state concentration in H_2 containing systems and in UO_2 containing systems (where the only reaction consuming H_2O_2 is the surface reaction with UO_2) is presented as a function of dose rate.

When comparing the H_2 induced reduction in steady-state concentration at different dose rates, it becomes evident that it increases with increasing dose rate. In fact, the ratio is inversely proportional to the square root of the dose rate according to Eq. (10).

$$\frac{[H_2O_2]_{S-S(H_2)}}{[H_2O_2]_{S-S}} = \left(0.026 \frac{1}{\sqrt{\dot{D}}} + 0.005\right) \tag{10}$$

This expression can also be derived directly from the dose rate dependence of the two individual steady-state expressions. It is important to note that Eq. (10) is only valid above the critical H_2 pressure. Since the dose rate decreases with distance from the fuel surface and since the relative effect of H_2 increases with dose rate, the relative effect of H_2 will decrease with increasing distance from the surface. The direct consequence of this is that the effective dose rate profile will change shape into a less pronounced gradient. The impact of the radiolytic H_2 effect can be estimated by integrating the dose rate profile [25] taking the dose rate dependent H_2 effect into account. From this estimation, it is clear that the reduction in H_2O_2 steady-state concentration follows the same relationship as Eq. (10) using the average dose rate for a given profile. When applying this to a hypothetical case of 38 MWd/kg burn-up fuel of different ages, we estimate the relative steady-state concentration ratios to be 0.08, 0.16, 0.34 and 1 for fuel ages 100, 1000, 10,000 and 100,000 years, respectively. Hence, the impact of the radiolytic H_2 effect decreases with increasing fuel age. From this elaboration, we can conclude that the radiolytic H_2 effect can be accounted for also in the steady-state approach. If we only take the actual inhibition of matrix dissolution (excluding the reduction of dissolved U(VI)) into account, the following equation (derived from Eqs. (8) and (10)) can be used to estimate the rate of radiation induced dissolution of UO_2 in the H_2 pressure range 1–40 bar.

$$r_{diss} = \left(0.026 \frac{1}{\sqrt{\dot{D}}} + 0.005\right) \dot{D} G(H_2O_2) \rho \delta_{\max(\alpha)}) - k \varepsilon_{rel} [H_2] \tag{11}$$

The dose rate used in Eq. (11) is the average dose rate in the α-irradiated volume. Both in the case of spent nuclear fuel and α-doped UO_2, α-radiation is not the only type of ionizing radiation emitted from the solid. Spent nuclear fuel contains β- and γ-emitters and most α-decays are accompanied by emission of γ-photons. Hence, α-doped UO_2 is not a pure source of α-radiation. The γ-dose rate is significantly lower than the α-dose rate but a much larger volume is affected by γ-radiolysis. Furthermore, the *G*-values for production of radicals are much higher in the case of β- and γ-radiolysis compared to α-radiolysis. Hence, radiation induced reduction of U(VI) is expected to be more powerful in β- and γ-irradiated solutions containing H_2. In Fig. 8, the U(VI) concentration is plotted as a function of irradiation time for γ-dose rates in the range of 1.6×10^{-8}–1.6×10^{-5} Gy s^{-1}. The HCO_3^- concentration used in the simulations is 10^{-3} mol dm^{-3} and the H_2 pressure is 1 bar. The initial U(VI) concentration is 10^{-7} mol dm^{-3}.

Obviously, even these low dose rates are sufficient to reduce the U(VI) concentration to very low levels at fairly low H_2 pressure. It should be pointed out that the volume affected by γ-radiolysis is several orders of magnitude larger than the volume affected by

Table 4
Ratios between H_2O_2 steady-state concentrations under H_2 and in UO_2 systems.

	0.000544 Gy s^{-1}	0.0059 Gy s^{-1}	0.0287 Gy s^{-1}	0.119 Gy s^{-1}	0.595 Gy s^{-1}
40 bar H_2	1.14	0.35	0.16	0.08	0.04

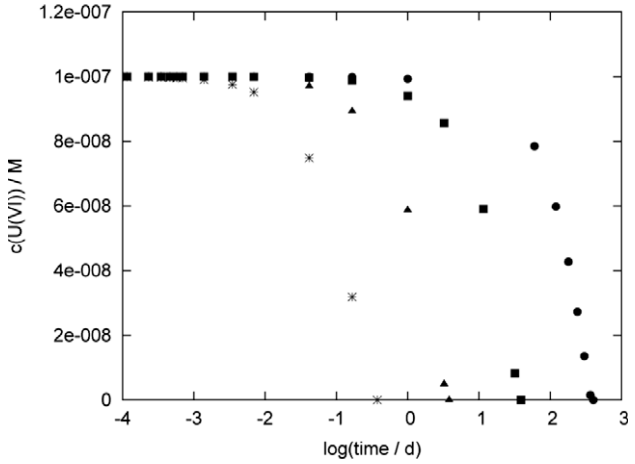

Fig. 8. U(VI) concentration as function of the logarithm of the γ-irradiation time at 1.6×10^{-8} (●), 1.6×10^{-7} (■), 1.6×10^{-6} (▲), 1.6×10^{-5} (∗) Gy s^{-1}.

α-radiolysis. Hence, the impact of H_2 in combination with low γ-dose rates on dissolved U(VI) is expected to be considerable. This is a plausible explanation of the H_2 effect observed in several leaching studies using α-doped UO_2 [13,14]. However, it should be noted that the precise magnitude of this effect is somewhat uncertain given the uncertainty in some of the rate constants used in the simulations. The α-radiation induced H_2 effect alone is not sufficient to explain the experimental observations. In the majority of the cases, the conditions (dose rate, H_2 pressure and HCO_3^- concentration) are outside the range where low steady-state concentrations of U(VI) are expected. It should be stressed that the rate of uranium concentration decrease in solution is probably somewhat lower than indicated by Fig. 8. The main reason for this is that aggregation and sedimentation of colloidal U(IV) particles will delay the disappearance of uranium from solution.

4. Conclusions

In this work, we have investigated the effect of H_2 on the H_2O_2 concentration during α-radiolysis using numerical simulations. The effect of dose rate, H_2 pressure and HCO_3^- concentration on the H_2O_2 concentration as well as the concentration of U(VI) in solution has been studied. The impact of H_2 is found to be strongly dose rate dependent, and this dependence explains the somewhat puzzling experimental data previously published by Pastina and LaVerne. This also verifies the reliability of the reaction scheme used in most numerical simulations of aqueous radiolysis. From the systematic variation of the dose rate, H_2 pressure and HCO_3^- concentration, the following conclusions can be drawn:

- At sufficiently high H_2 pressures, the H_2O_2 concentration reaches steady-state upon α-radiolysis.
- The critical H_2 pressure required to suppress the H_2O_2 concentration during α-radiolysis as well as the steady-state concentration of H_2O_2 are strongly dose rate dependent.
- The steady-state concentration of H_2O_2 is also dependent on the H_2 pressure.
- The steady-state concentration of the hydrogen atom governs the steady-state concentration of H_2O_2, and both steady-state concentrations follow similar H_2 pressure and dose rate dependences.
- Due to the α-radiolytic H_2 effect, the steady-state concentration of H_2O_2 is lower than the H_2O_2 steady-state concentration expected in α-radiation induced dissolution of spent nuclear fuel in the absence of H_2. Consequently, H_2 will reduce the rate of α-radiation induced dissolution of spent nuclear fuel.
- The α-radiolytic H_2 effect can easily be accounted for in the steady-state approach for predictive modeling of radiation induced dissolution of spent nuclear fuel.
- Hydrogen atoms produced upon α-radiolysis of H_2 containing water will also reduce the uranium concentration in solution. This process is efficient only at higher dose rates and cannot explain the H_2 effect observed in many experiments on α-doped UO_2.
- Low γ-dose rate in combination with moderate H_2 pressure is efficiently reducing U(VI) in solution. This is the probable reason for the low U(VI) concentrations observed in leaching experiments on α-doped UO_2 in the presence of H_2.

Acknowledgement

The Swedish Nuclear Fuel and Waste Management Co. (SKB) is gratefully acknowledged for financial support.

References

[1] D.W. Shoesmith, J. Nucl. Mater. 282 (2000) 1–31.
[2] R.L. Segall, R.S.C. Smart, P.S. Turner, Oxide surfaces in solution, in: J. Nowotny, L.-C. Durfour (Eds.), Surface and Near-Surface Chemistry of Oxide Materials, Elsevier, Amsterdam, 1988.
[3] J.W.T. Spinks, R.J. Woods, An Introduction to Radiation Chemistry, third ed., John Wiley & Sons Inc., New York, 1990.
[4] E. Ekeroth, O. Roth, M. Jonsson, J. Nucl. Mater. 355 (2006) 38–46.
[5] M. Jonsson, F. Nielsen, O. Roth, E. Ekeroth, S. Nilsson, M.M. Hossain, Environ. Sci. Technol. 41 (2007) 7087–7093.
[6] F. Nielsen, M. Jonsson, J. Nucl. Mater. 374 (2008) 281–285.
[7] D. Cui, E. Ekeroth, P. Fors, K. Spahiu, Mat. Res. Soc. Sympos. Proc. 1104 (2008) 87–99.
[8] S. Röllin, K. Spahiu, U.-B. Eklund, J. Nucl. Mater. 297 (2001) 231–243.
[9] P. Carbol, J. Cobos-Sabathe, J.-P. Glatz, C. Ronchi, V. Rondinella, D. H. Wegen, T. Wiss, A. Loida, V. Metz, B. Kienzler, K. Spahiu, B. Grambow, J. Quinones, A.M.E. Valiente, Tech. Rep. TR-05-09, Svensk Kärnbränslehantering AB, March 2005.
[10] M.E. Broczkowski, J.J. Noel, D.W. Shoesmith, J. Nucl. Mater. 346 (2005) 16–23.
[11] M. Trummer, S. Nilsson, M. Jonsson, J. Nucl. Mater. 378 (2008) 55–59.
[12] T.E. Eriksen, M. Jonsson, J. Merino, J. Nucl. Mater. 375 (2008) 331–339.
[13] B. Muzeau, C. Jégou, F. Delaunay, V. Broudic, A. Brevet, H. Catalette, E. Simoni, C. Corbel, J. Alloys Compd. 467 (2009) 578–589.
[14] P. Carbol, P. Fors, T. Gouder, K. Spahiu, Geochim. Cosmochim. Acta 73 (2009) 4366–4375.
[15] E.A.B. Ross, B.H.J. Bielski, G.V. Buxton, D.E. Cabelli, C.L. Greenstock, W.P. Helman, R.E. Huie, J. Grodkowski, P. Neta, NDRL/NIST Solution Kinetics Database, 1992. (and references therein).
[16] R.D. Saini, P.K. Bhattacharyya, Radiat. Phys. Chem. 29 (1987) 375–379.
[17] A.V. Gogolev, V.P. Shilov, A.M. Fedoseev, A.K. Pikaev, Radiat. Phys. Chem. 37 (1991) 531–535.
[18] N.S. Guha, P.N. Moorthy, K.N. Rao, Radiat. Phys. Chem. 29 (1987) 425–428.
[19] B. Pastina, J.A. LaVerne, J. Phys. Chem. A 105 (2001) 9316–9322.
[20] M.B. Carver, D.V. Hanley, K.R. Chaplin, MAKSIMA-CHEMIST a Program for Mass Action Kinetics Simulation by Automatic Chemical Equation Manipulation and Integration Using Stiff Techniques, Atomic Energy of Canada Limited, Chalk River Nuclear Laboratories, Ontario, 1979.
[21] J.C. Sullivan, S. Gordon, D. Cohen, W. Mulac, K.H. Schmidt, J. Phys. Chem. 80 (1976) 1684–1686.
[22] M.M. Hossain, E. Ekeroth, M. Jonsson, J. Nucl. Mater. 358 (2006) 202–208.
[23] T.E. Eriksen, H. Christensen, E. Bjergbakke, J. Radioanal. Nucl. Chem. 116 (1987) 13–25.
[24] G. Choppin, J.O. Liljenzin, J. Rydberg, Radiochemistry and Nuclear Chemistry, Reed Educational and Professional Publishing Ltd., Oxford, 1995.
[25] F. Nielsen, M. Jonsson, J. Nucl. Mater. 359 (2006) 1–7.
[26] J.A. LaVerne, R.H. Schuler, J. Phys. Chem. 91 (1987) 5770–5776.
[27] E. Ekeroth, M. Jonsson, T.E. Eriksen, K. Ljungqvist, S. Kovács, I. Puigdomenech, J. Nucl. Mater. 334 (2004) 35–39.
[28] F.A. Forward, J. Halpern, Can. Min. Metall. Bull. 56 (1953) 645.